Electronic Supplementary Information

Safeguarding RuO_2 phase against lattice oxygen oxidation during acidic water electrooxidation

Haneul Jin,[a,b†] Songa Choi,[a†] Gi Joo Bang,[c] Taehyun Kwon,[a,b] Hee Soo Kim,[b] Su Ji Lee,[b] Yongju Hong,[a] Dong Wook Lee,[b] Hyun S. Park,[b,d,e] Hionsuck Baik,[f] Yousung Jung,[c*] Sung Jong Yoo,[b,d,e*] and Kwangyeol Lee[a*]

[a] Department of Chemistry and Research Institute for National Science, Korea University, Seoul 02841, Republic of Korea

[b] Center for Hydrogen·Fuel Cell research, Korea Institute of Science and Technology (KIST), Seoul 02792, Republic of Korea

[c] Department of Chemical and Biomolecular Engineering (BK21 four), Korea Advanced Institute of Science and Technology (KAIST), Daejeon 34141, Republic of Korea

[d] Division of Energy & Environment Technology, KIST School, University of Science and Technology (UST), Seoul 02792, Republic of Korea

[e] KHU-KIST Department of Converging Science and Technology, Kyung Hee University, Seoul 02447, Republic of Korea

[f] Korea Basic Science Institute (KBSI), Seoul 02841, Republic of Korea

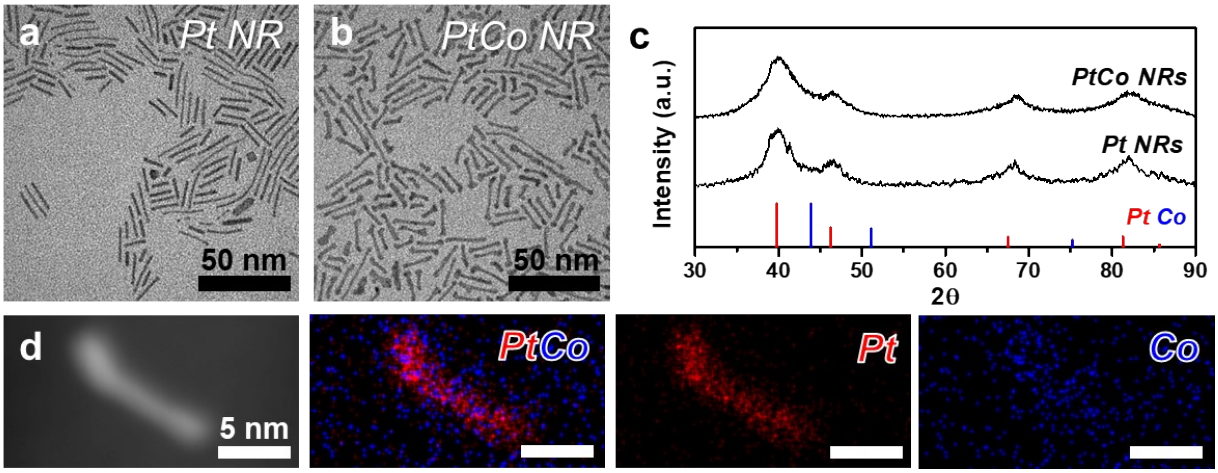

Fig. S1 Characterization of Pt-based nanorods as seeds. a-b) TEM images of Pt and PtCo nanorods, c) PXRD patterns of nanorods, and d) STEM image and corresponding elemental mapping of PtCo NR. Colored sticks in PXRD patterns representing diffraction lines for references: red for Pt (PDF#01-070-2057) and blue for Co (PDF#01-071-4238).

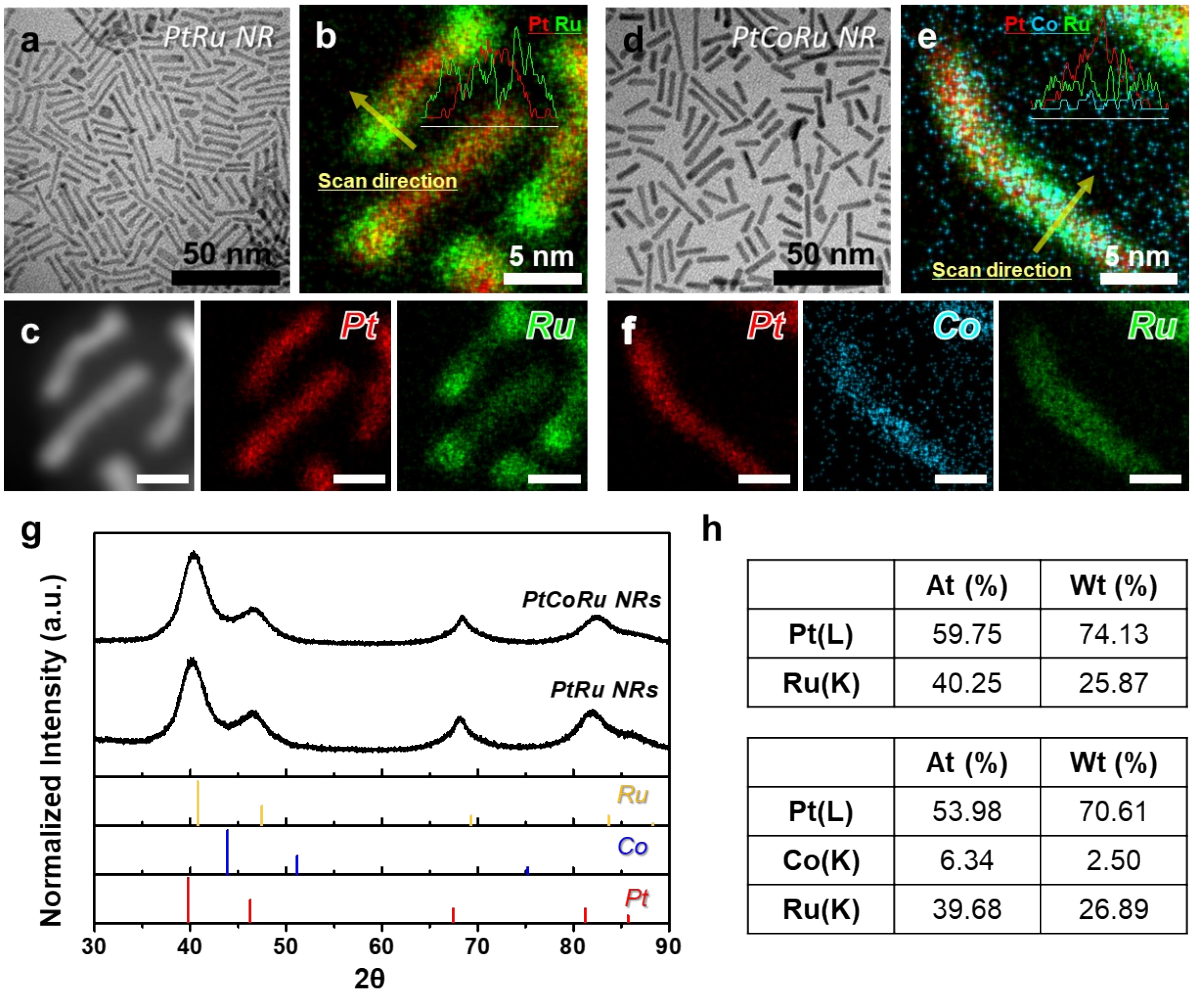

	At (%)	Wt (%)
Pt(L)	59.75	74.13
Ru(K)	40.25	25.87

	At (%)	Wt (%)
Pt(L)	53.98	70.61
Co(K)	6.34	2.50
Ru(K)	39.68	26.89

Fig. S2 Representative TEM images and elemental mapping analyses of a-c) PtRu NR and d-f) PtCoRu NR. Scale bars in c) and f) indicate 5 nm. g) PXRD patterns of each nanorod. Colored sticks in PXRD patterns representing diffraction lines for references: red for Pt (PDF#01-070-2057), blue for Co (PDF#01-071-4238), and yellow for Ru (PDF#01-088-2333). h) atomic compositions obtained by EDS for PtRu NR (top) and PtCoRu NR (bottom), respectively.

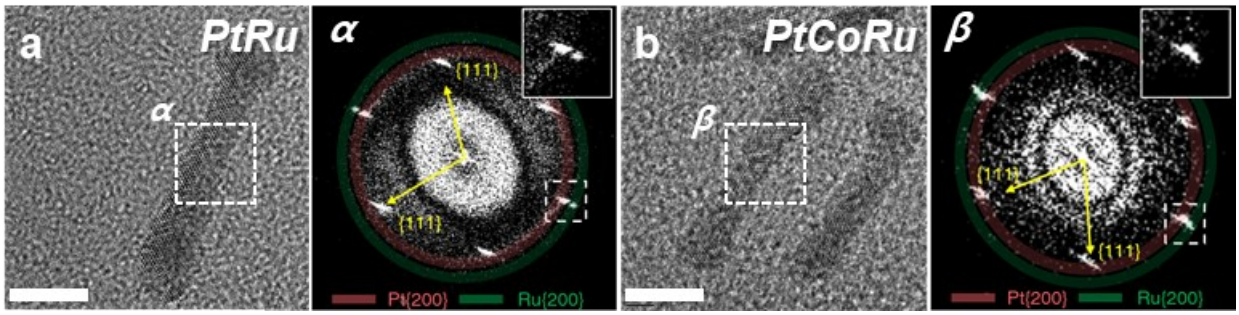

Fig. S3 HRTEM images (a and b) and corresponding FFT patterns (α and β) of PtRu and PtCoRu NRs, respectively. Green circle and red circle represent *d*-spacing range of Ru{200} and Pt{200}, respectively. Yellow arrows represent Pt{111}. The scale bars are 5 nm.

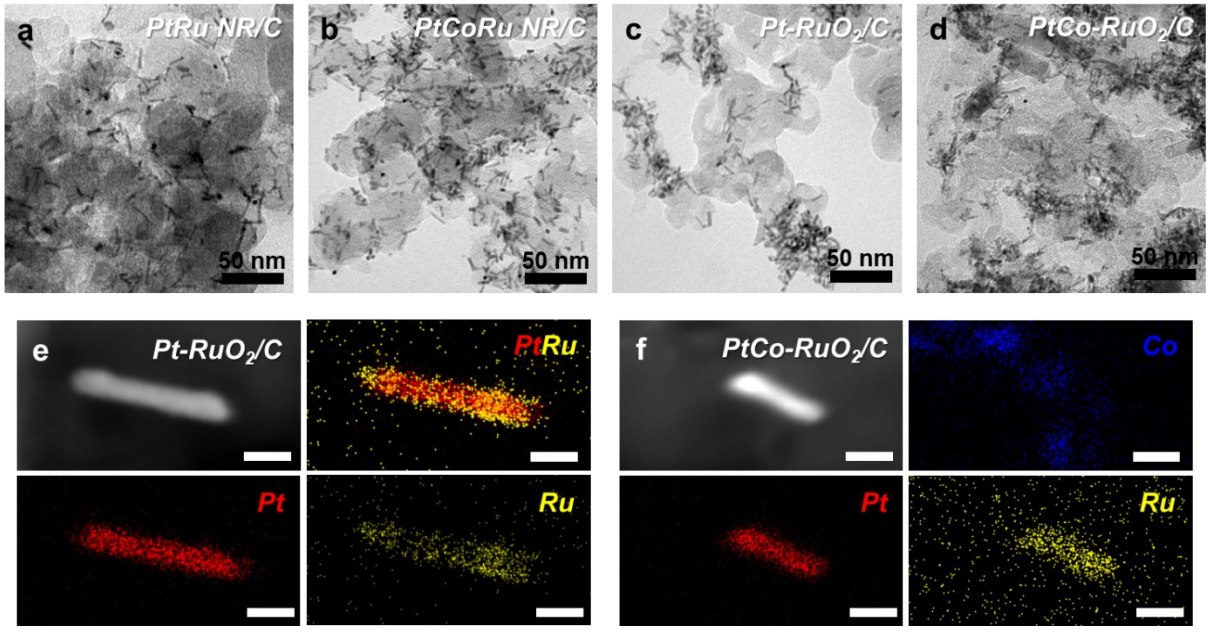

Fig. S4 TEM images of each nanorod loaded on carbon support (Vulcan XC-72). a) PtRu NR/C, b) PtCoRu NR/C, c) Pt-RuO_2/C, and d) PtCo-RuO_2/C. STEM images and corresponding elemental mapping images of e) Pt-RuO_2/C and f) PtCo-RuO_2/C. Scale bars in Fig. S5e-f indicate 5 nm.

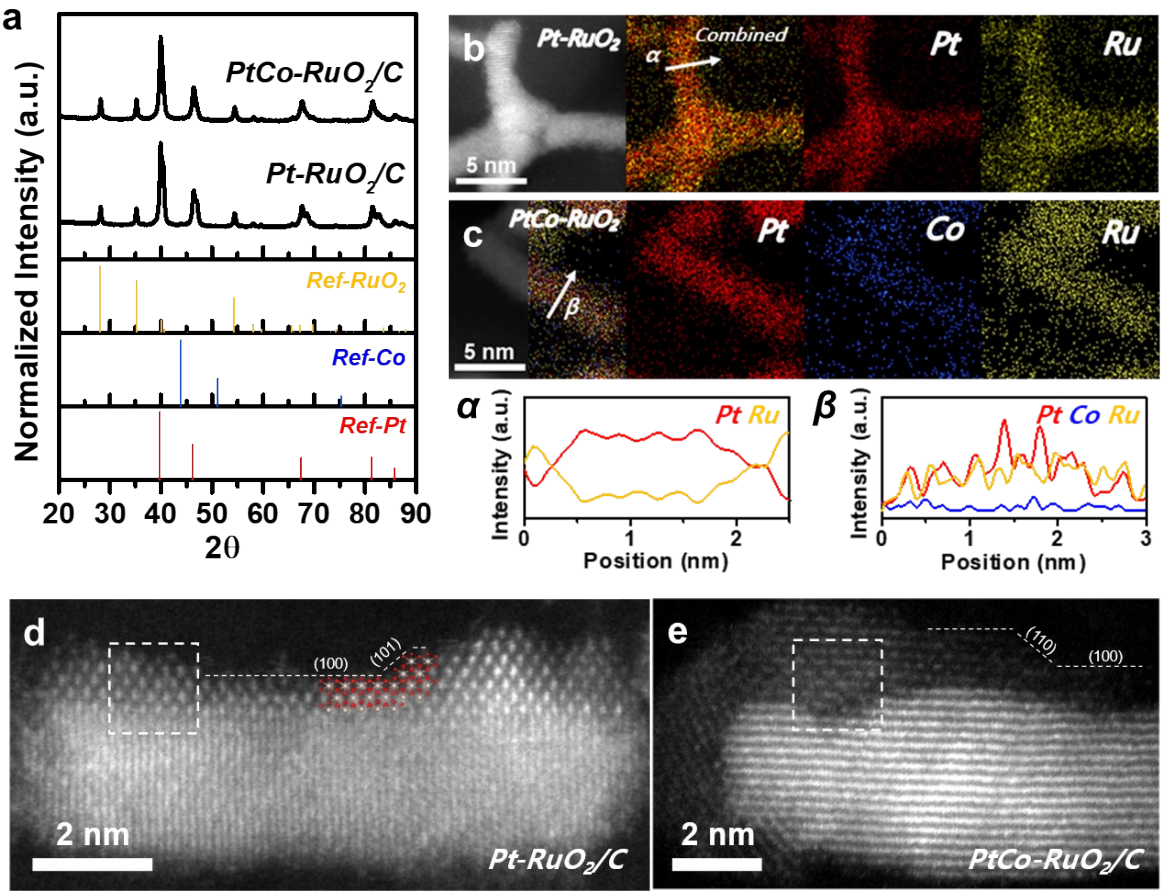

Fig. S5 a) Powder XRD patterns, b-c) HRSTEM images, and corresponding elemental mapping images of Pt-RuO_2/C and PtCo-RuO_2/C, respectively. Elemental mapping images and line scan profiles (α and β) with vertical direction through NRs showed well-distributed Pt, Ru, and Co in PtCo-RuO_2/C, while Ru-rich shell region is observed in the Pt-RuO_2/C, indicating that a significant amount of Pt atoms is impregnated in the RuO_2 shell. d-e) High resolution dark field images of d) Pt-RuO_2/C and e) PtCo-RuO_2/C**.**

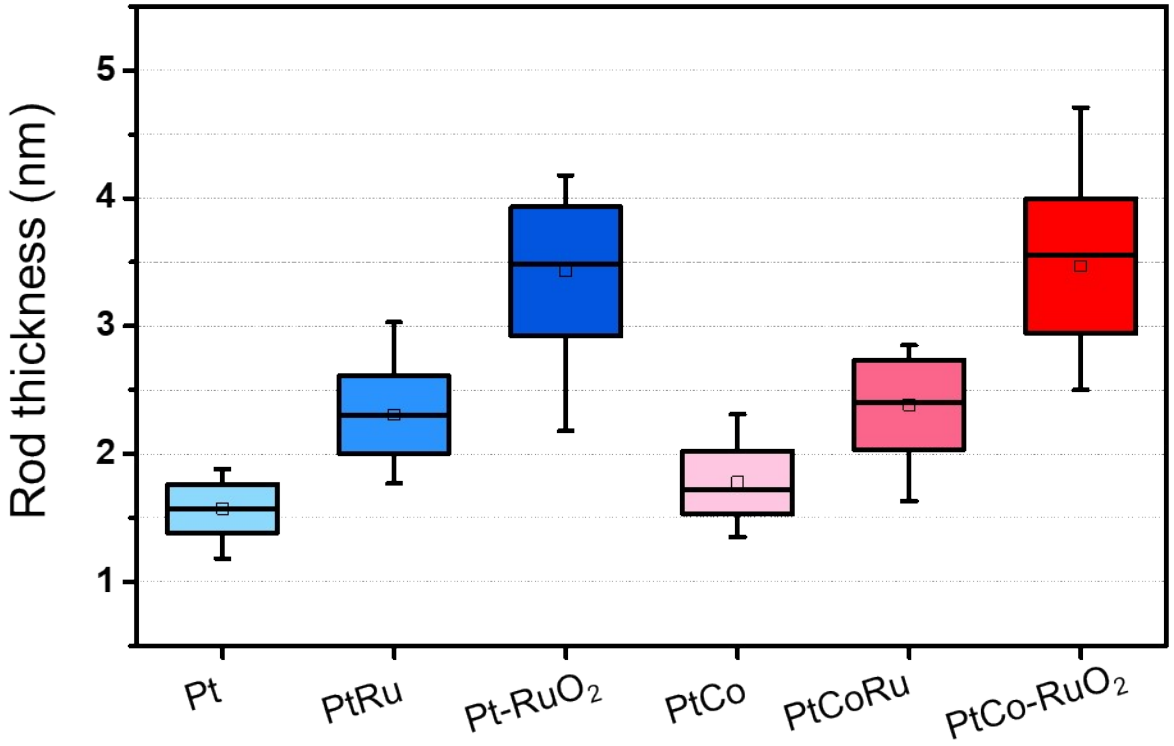

Fig. S6 Size distribution of Pt-based seeds and nanorods with Ru and RuO_2 shells

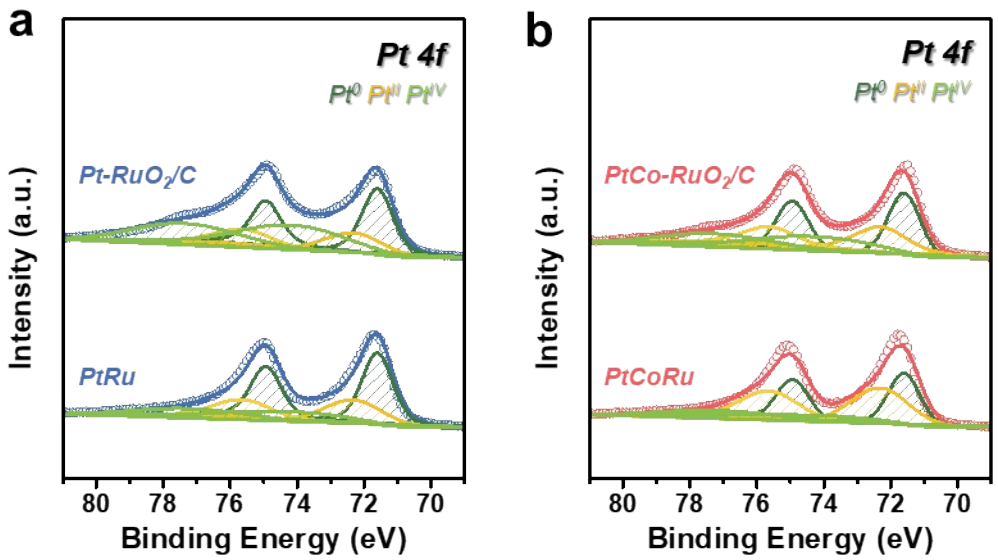

Fig. S7 Pt 4f XPS of a) PtRu-based catalysts and b) PtCoRu-based catalysts of before and after thermal oxidation.

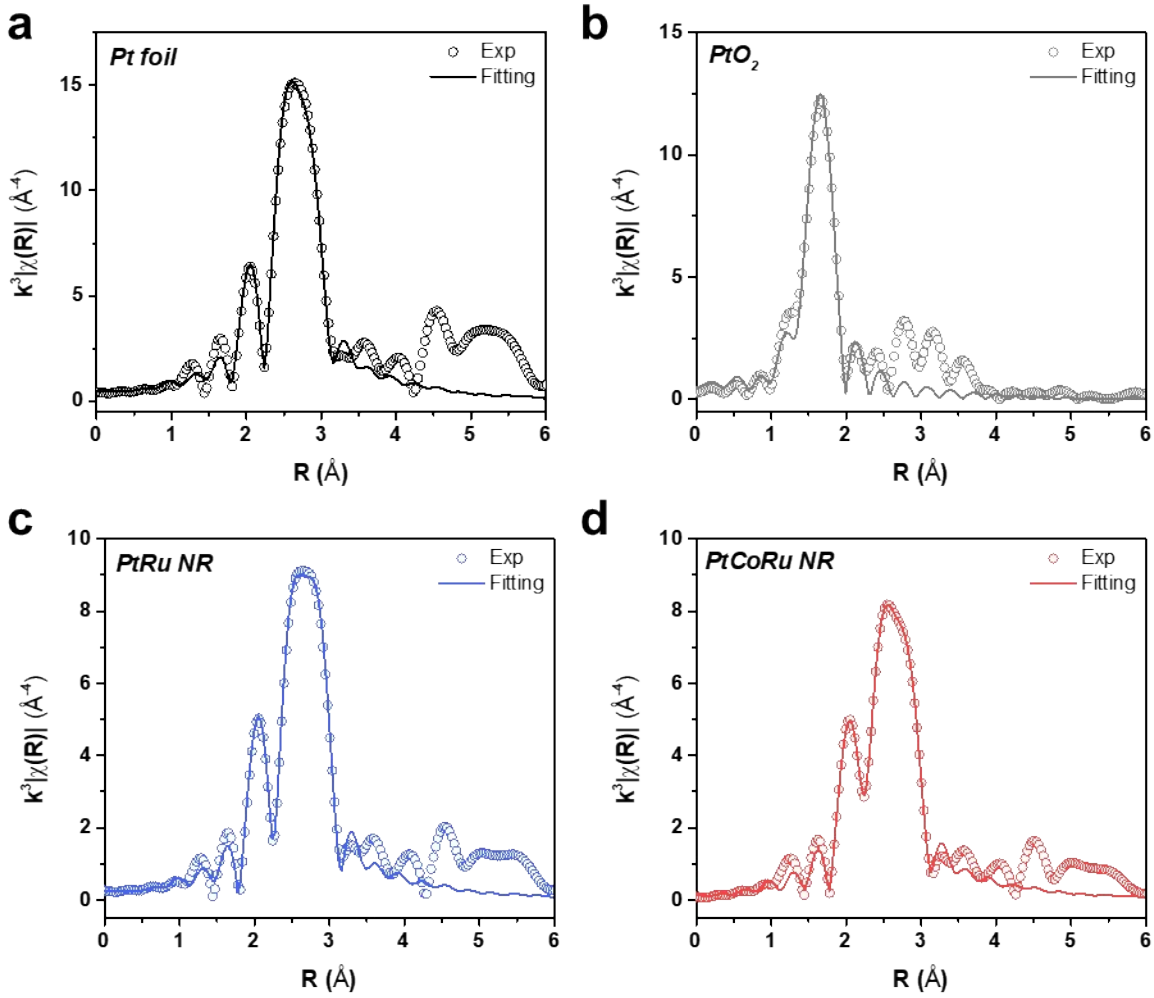

Fig. S8 Pt L_3-edge FT-EXAFS spectra in R-space with fitting curves of a) Pt foil (fitting range: R = 1.2-3.0 Å), b) PtO_2 (fitting range: R = 1.2-2.2 Å), c) PtRu NR (fitting range: R = 1.2-3.2 Å), and d) PtCoRu NR (fitting range: R = 1.2-3.2 Å).

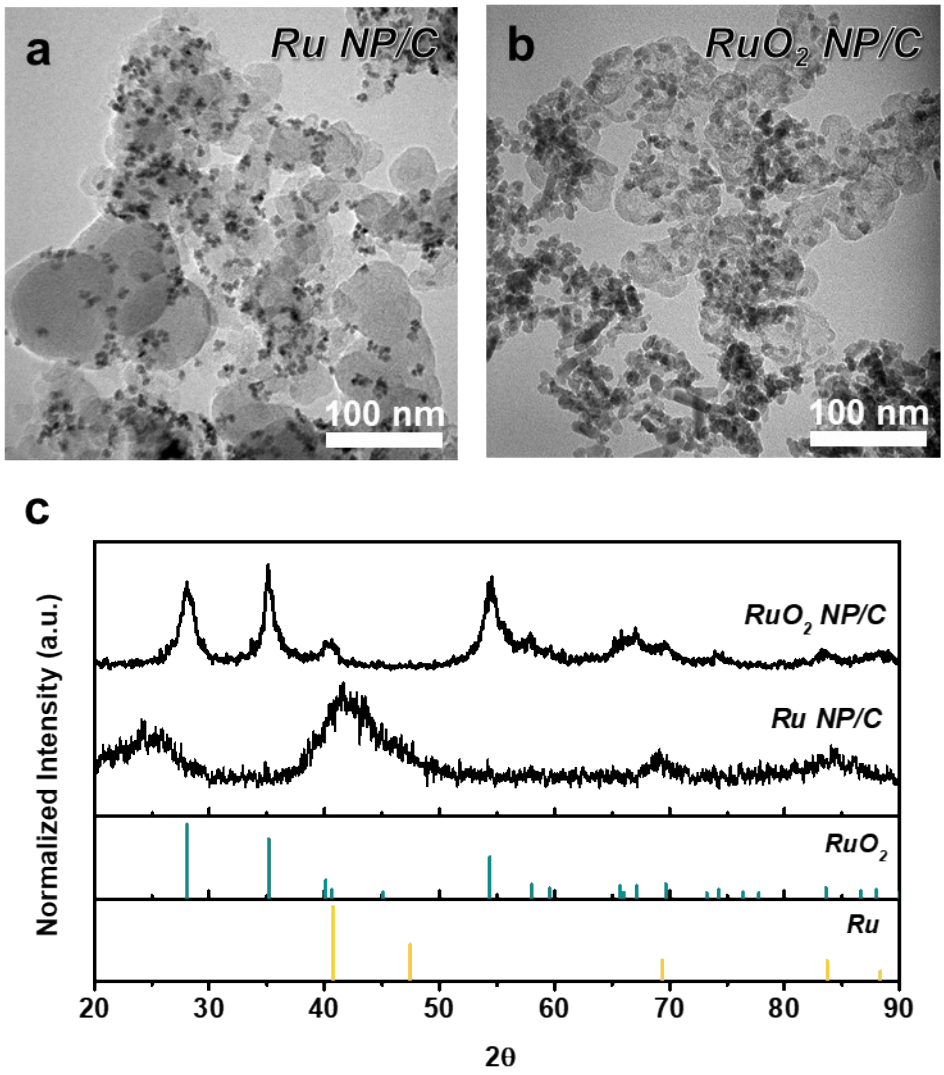

Fig. S9 TEM images of home-made a) Ru NP/C and b) RuO_2 NP/C. c) PXRD patterns of Ru NP/C and RuO_2 NP/C. Colored sticks in PXRD patterns indicate references: yellow for Ru (PDF#01-088-2333) and dark cyan for RuO_2 (PDF#01-075-4303).

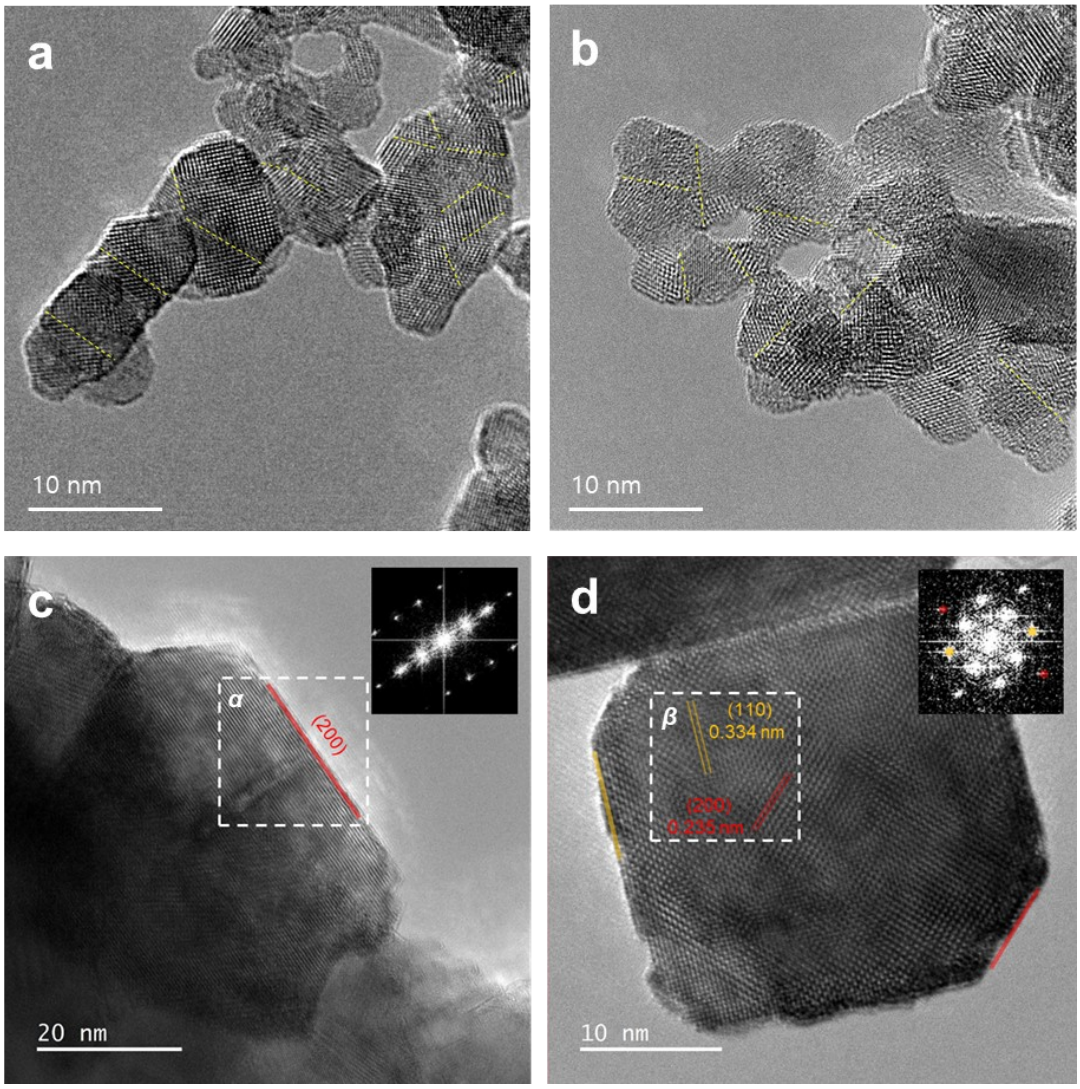

Fig. S10 HRTEM images of home-made RuO_2 NP/C (a,b) and com. RuO_2/C (c,d), indicating that RuO_2 NP/C shows polycrystalline structure with multi-grains (yellow dashed line in Fig. S9a-b), while com. RuO_2/C with low-index facets shows a single crystalline phase. Inset images in c and d) indicate corresponding FFT patterns of α and β, respectively.

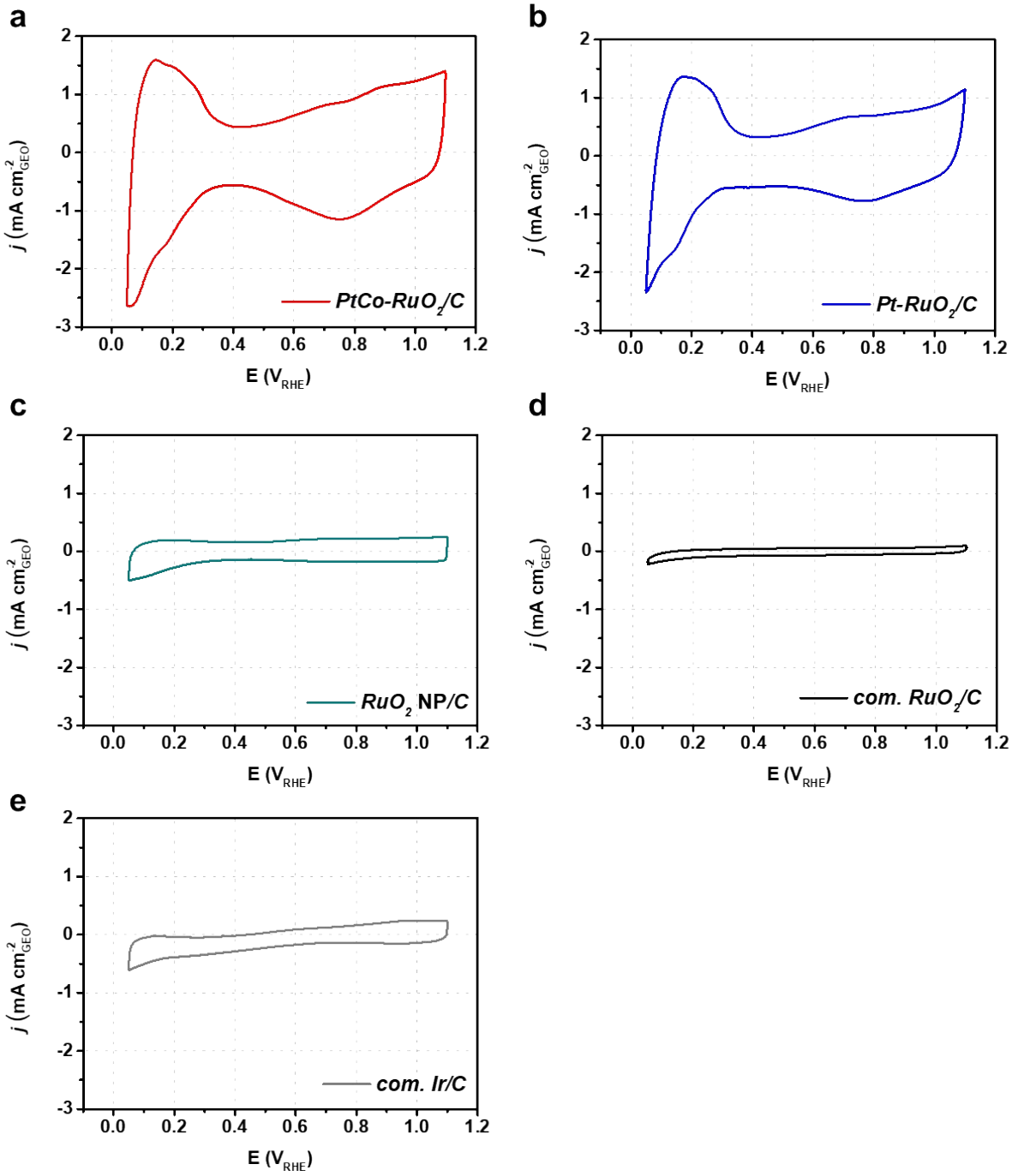

Fig. S11 Initial CV of the a) PtCo-RuO_2/C, b) Pt-RuO_2/C, c) RuO_2 NP/C, d) com. RuO_2/C, and e) com. Ir/C, measured from 0.05 to 1.1 V_{RHE} with 20 mV s^{-1} of scan rate.

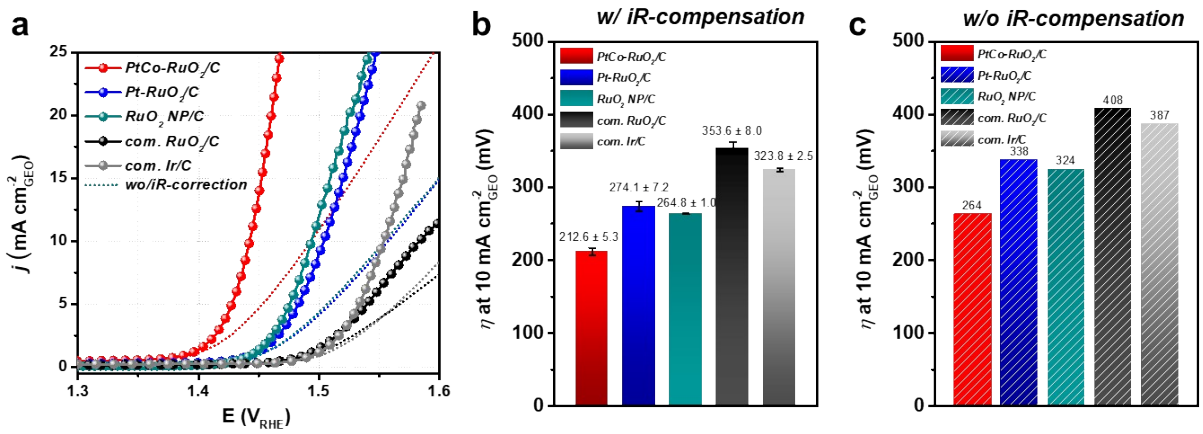

Fig. S12 a) LSV polarization curves with 100% iR-compensation (solid lines) and without iR-compensation (dotted lines). b-c) Bar graphs of overpotentials b) with iR-compensation and c) without iR-compensation at a current density of 10 mA cm^{-2}_{GEO}.

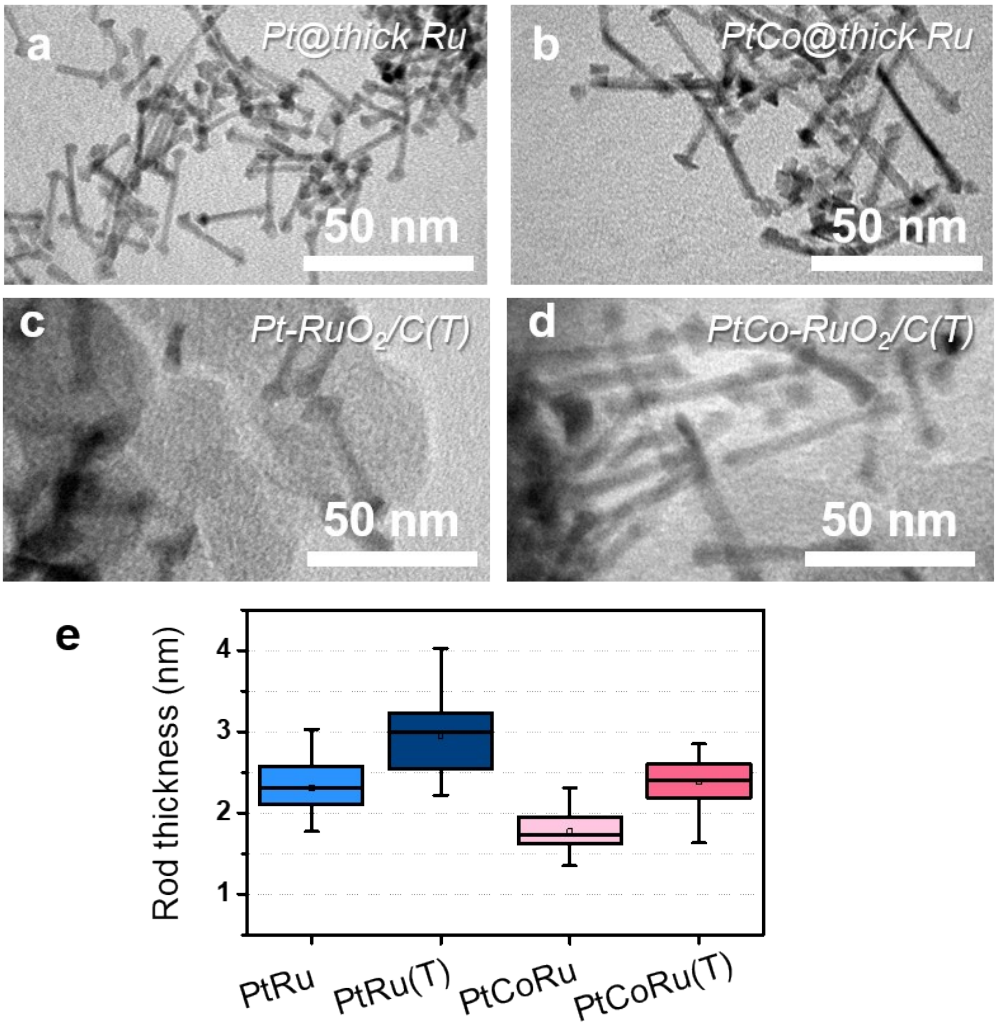

Fig. S13 TEM images of a) PtRu(T), b) PtCoRu(T), c) Pt-RuO_2/C(T), and d) PtCo-RuO_2/C(T), respectively. e) Size distribution of PtRu, PtRu(T), PtCo, and PtCoRu(T).

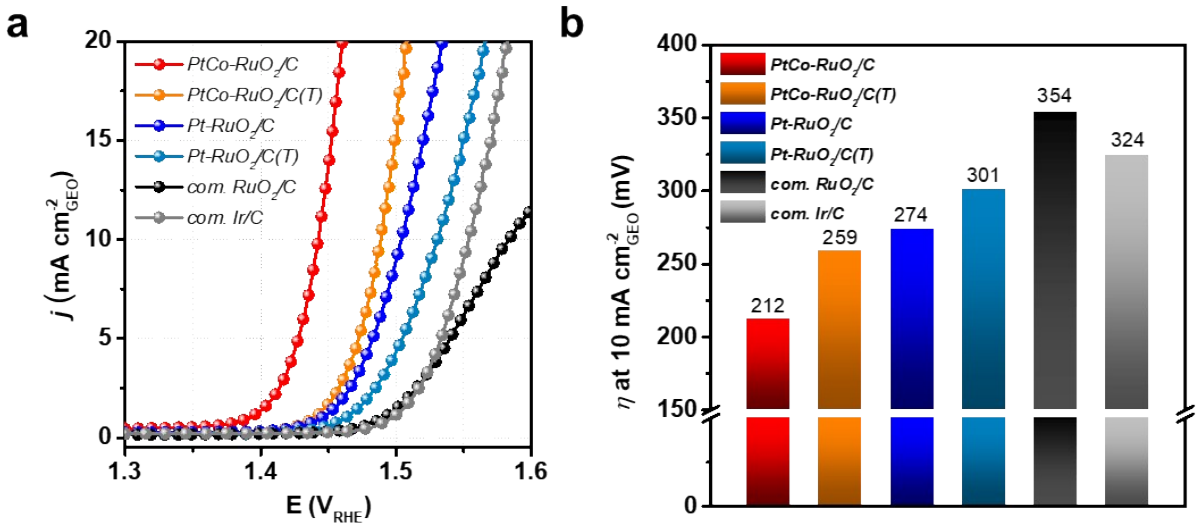

Fig. S14 Electrocatalytic performance of nanorods with optimized and thick RuO_2 shell. a) OER polarization curves and b) overpotential required at a current density of 10 mA cm^{-2}_{GEO}.

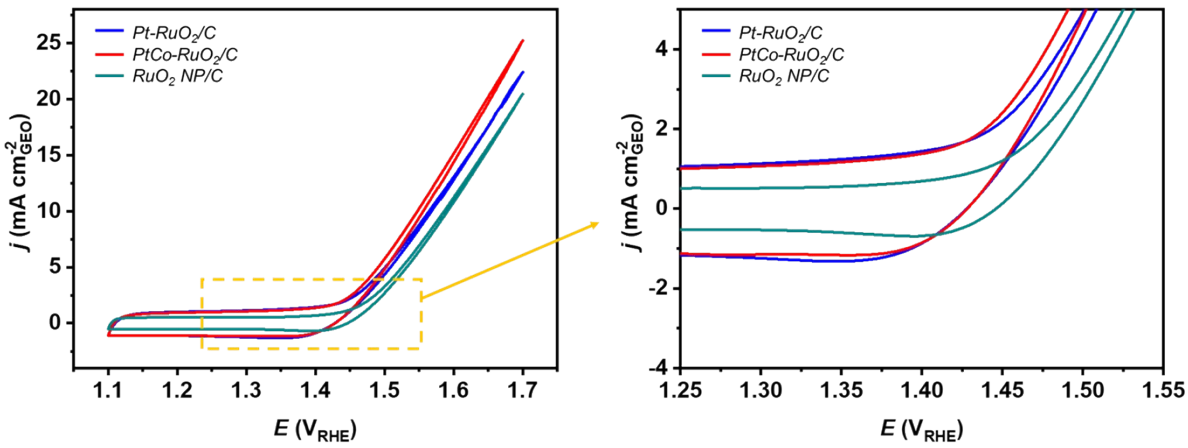

Fig. S15 CV scans of Pt-RuO_2/C, PtCo-RuO_2/C, and RuO_2 NP/C in OER potential ranges of 1.1-1.7 V_{RHE}.

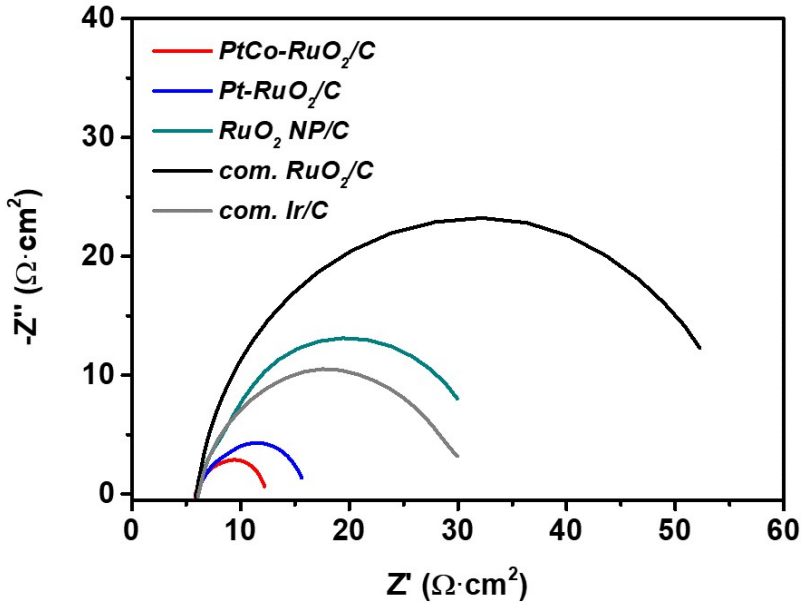

Fig. S16 ElS of different catalysts at 1.45 V_{RHE} in N_2-saturated 0.1 M $HClO_4$ solution.

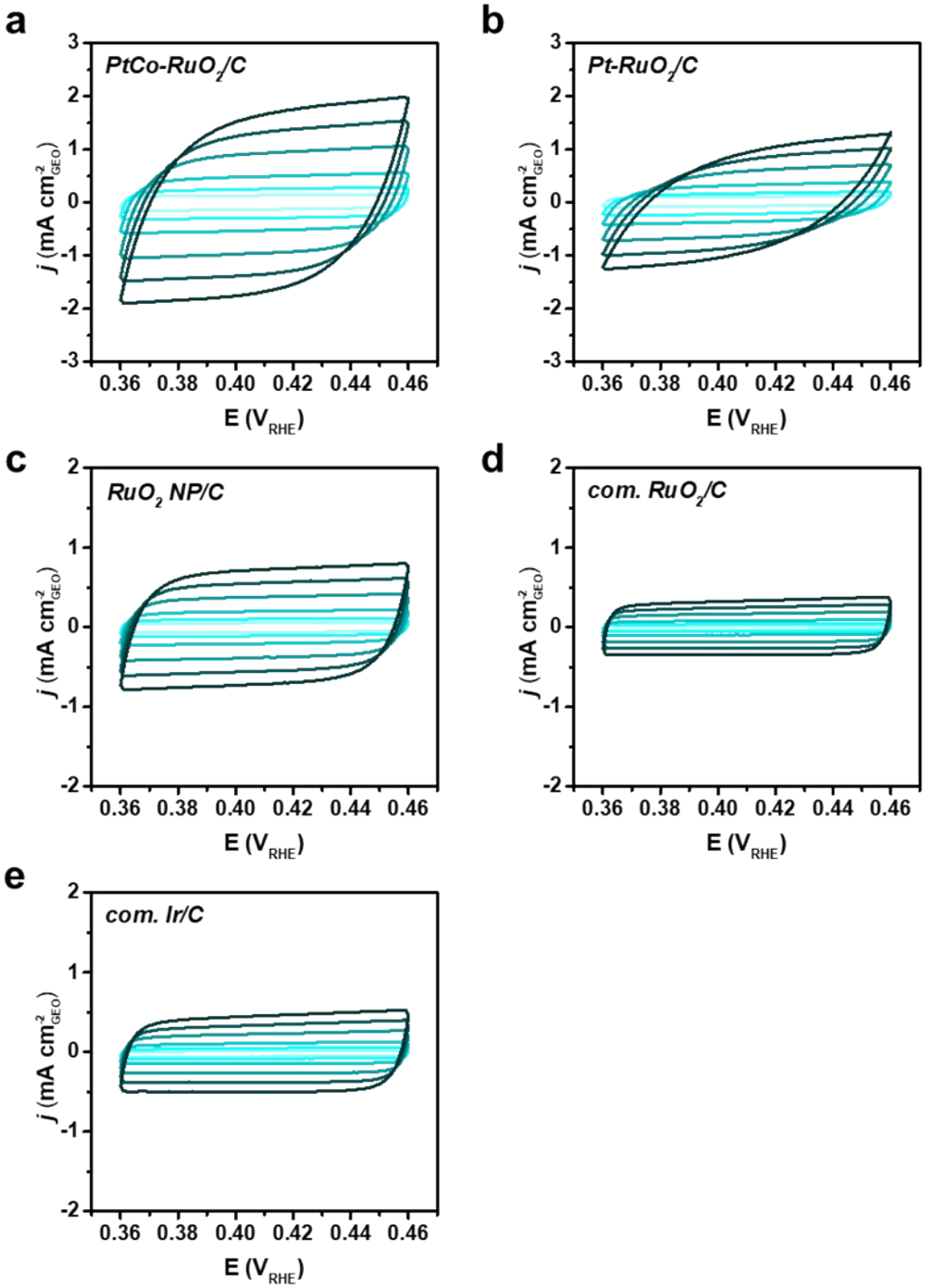

Fig. S17 CV curves for C_{dl} measured within the range from 0.36 to 0.46 V_{RHE} with scan rate from 10 to 160 mV s^{-1}.

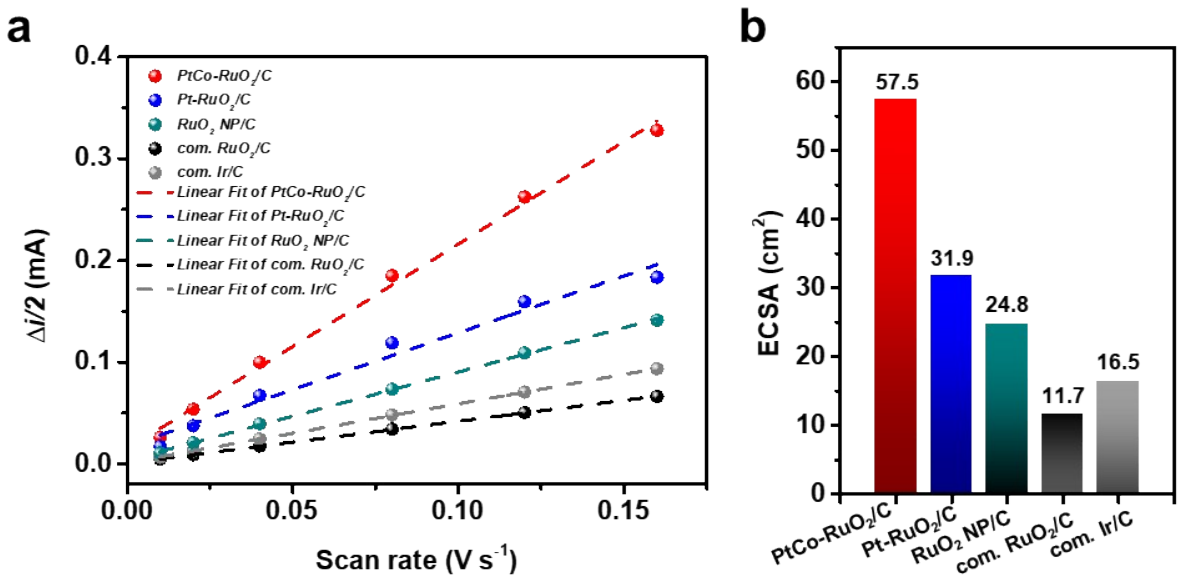

Fig. S18 a) Linear plots of capacitive current against scan rate. b) Bar graphs of ECSA for each catalyst.

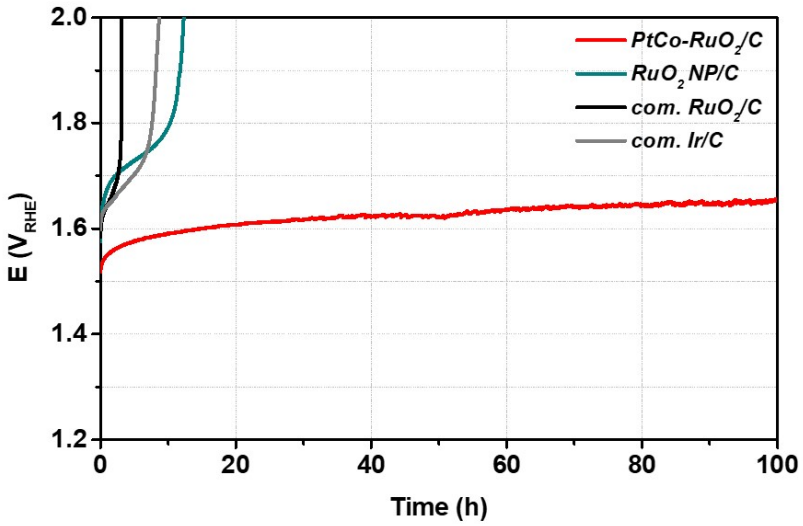

Fig. S19 OER chronopotentiometric test of PtCo-RuO_2/C at 10 mA cm^{-2}_{GEO} for 100 h.

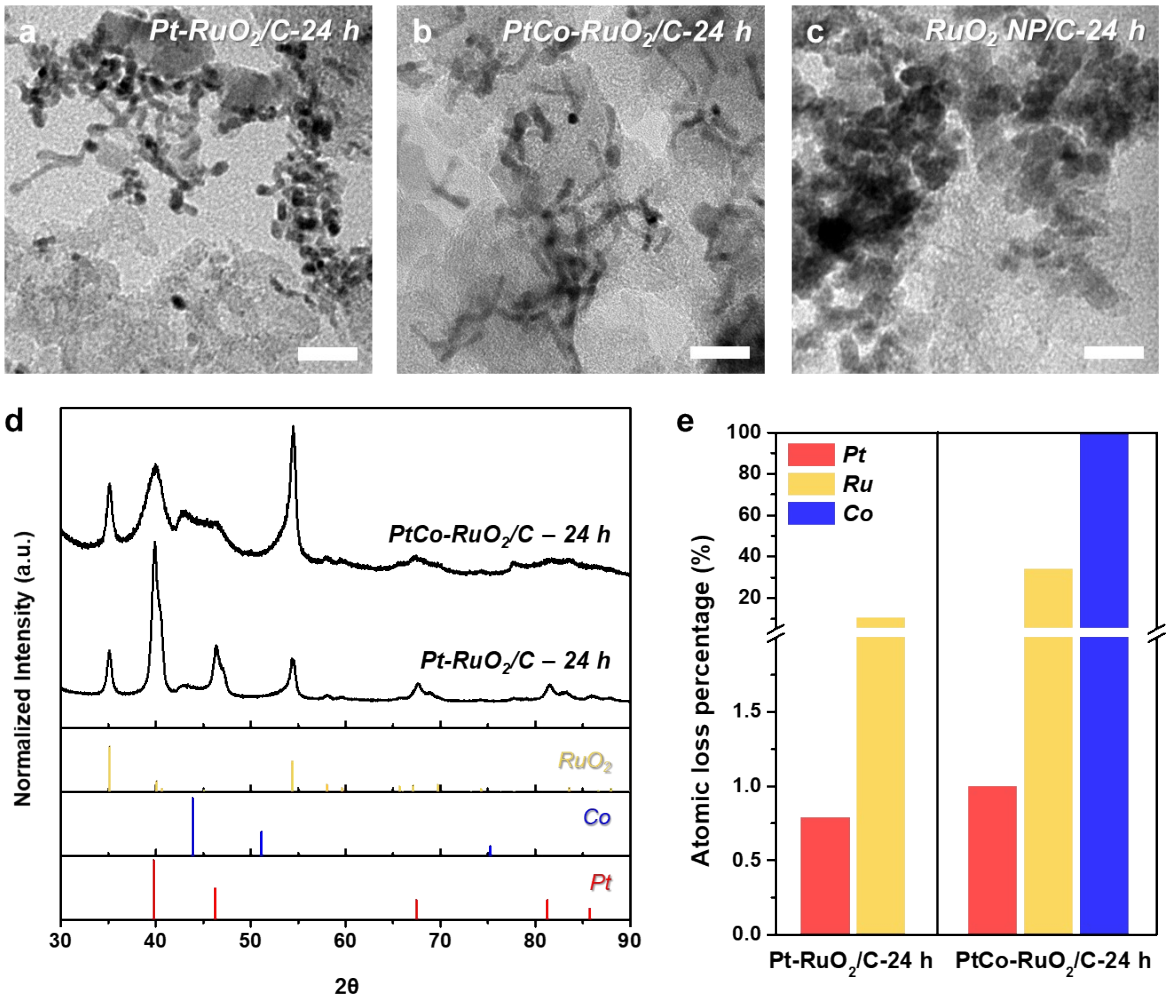

Fig. S20 TEM images of a) Pt-RuO_2/C-24 h, b) PtCo-RuO_2/C-24 h, and c) RuO_2 NP/C-24 h, which were obtained after 24 h of OER stability test. Scale bar in each TEM image indicates 20 nm. d) XRD patterns and e) bar graph of atomic loss percentage of catalysts after 24 h of OER. Atomic loss% were measured via analyzing electrolytes obtained after OER assessment using the ICP-MS.

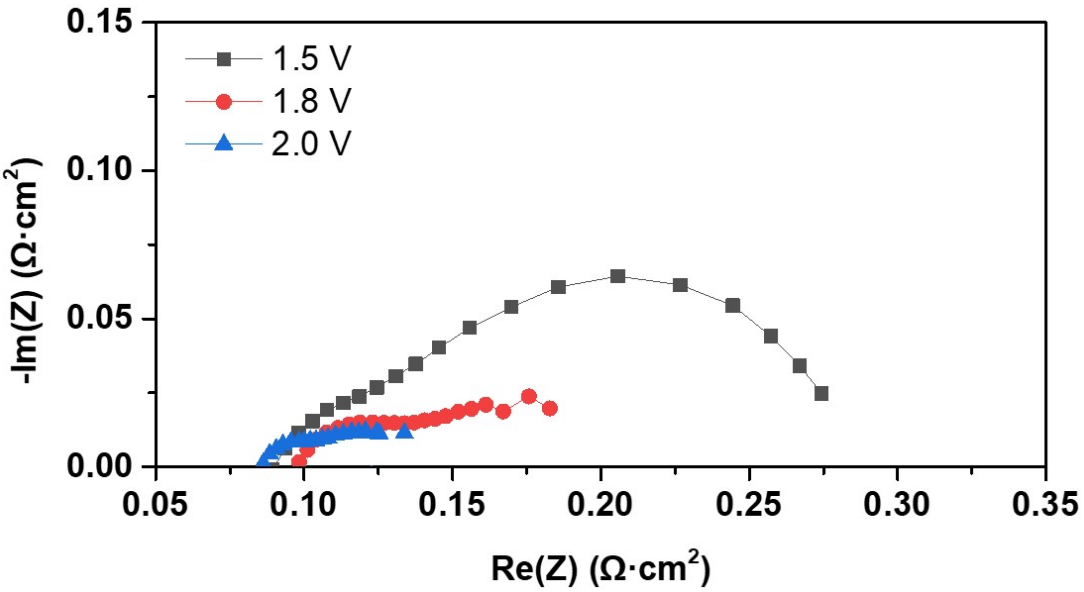

Fig. S21 EIS plots of PtCo-RuO_2/C in a MEA for water electrolysis at cell potentials of 1.5 V (black), 1.8 V (red), and 2.0 V (blue).

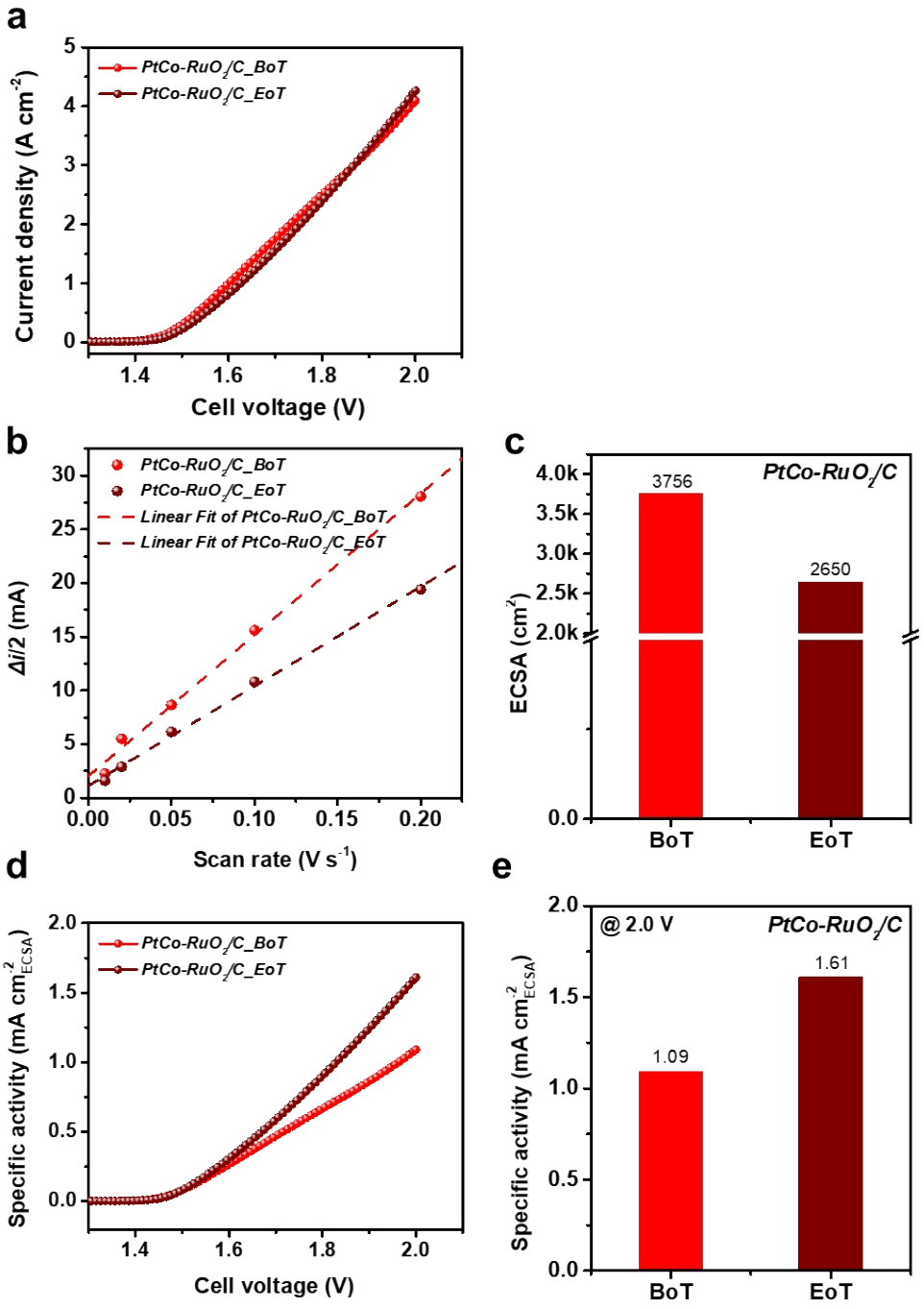

Fig. S22 a) LSV polarization curves of PtCo-RuO_2/C before and after CP test of 24 h for MEA, b) linear plots of capacitive current against scan rate, and c) bar graphs of ECSA for each catalyst. d) polarization curves for specific activity of of PtCo-RuO_2/C before and after CP test of 24 h for MEA and e) corresponding bar graphs of SA obtained at 2.0 V.

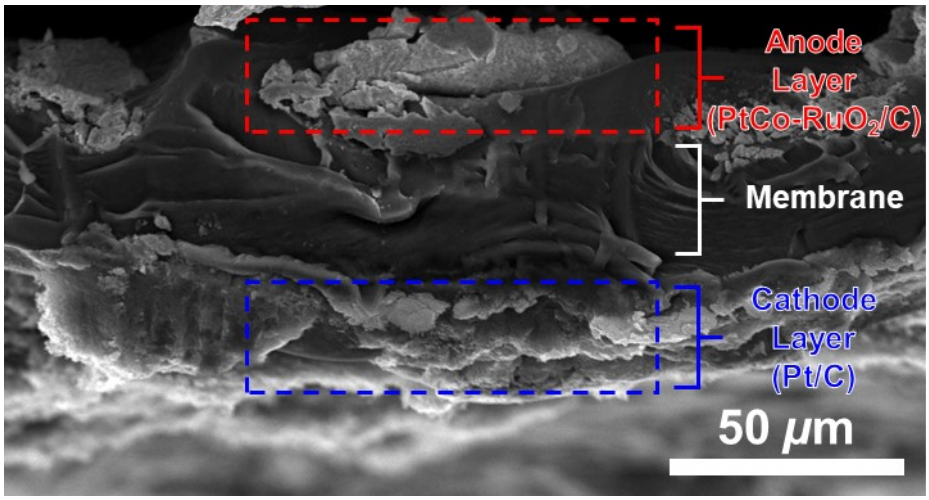

Fig. S23 Cross-sectional SEM image of MEA after long-term PEMWE operation.

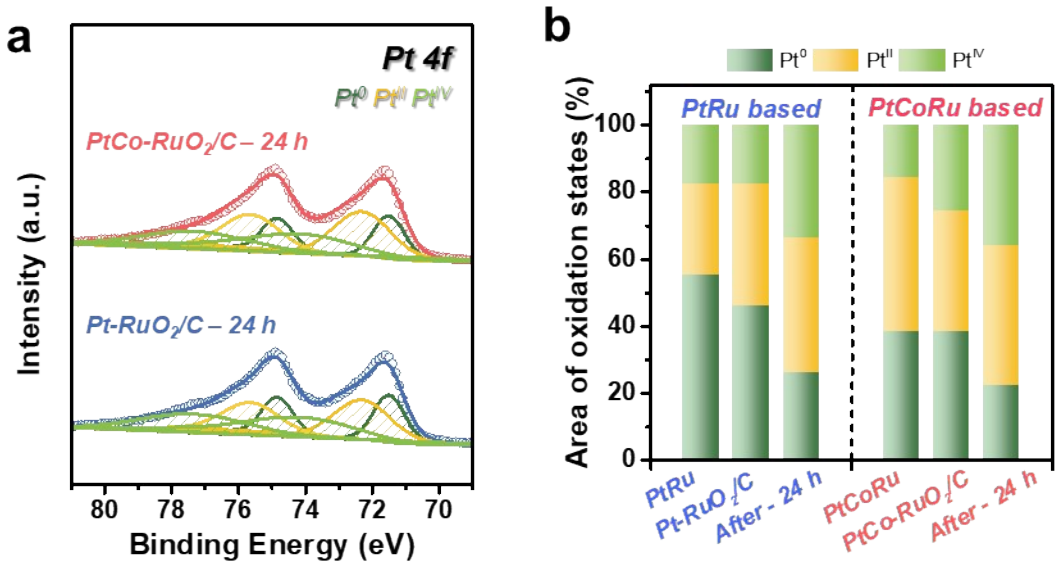

Fig. S24 a) Pt 4f XPS of PtRu-based catalysts and PtCoRu-based catalysts after OER stability test for 24 h. b) Area percentage of deconvoluted oxidation states for Pt 4f XPS of each catalyst before and after thermal oxidation, and after OER stability test.

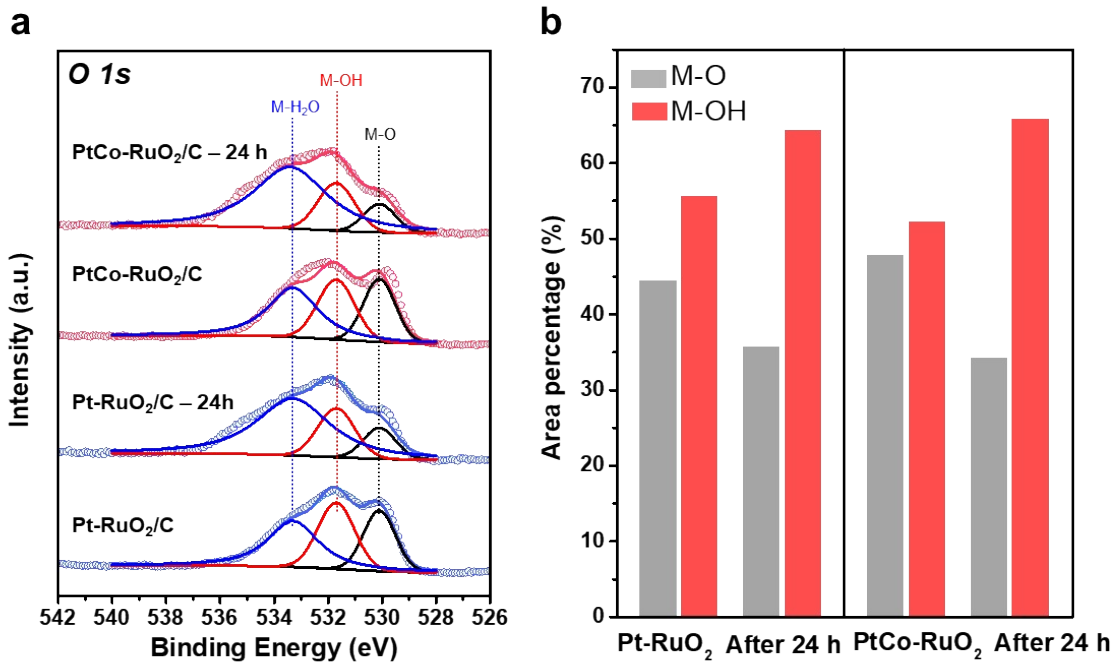

Fig. S25 a) O 1s XPS of PtRu-based catalysts and PtCoRu-based catalysts of before and after OER stability test for 24 h. b) Area percentage of deconvoluted M-O and M-OH for O 1s XPS of each catalyst (M = metal).

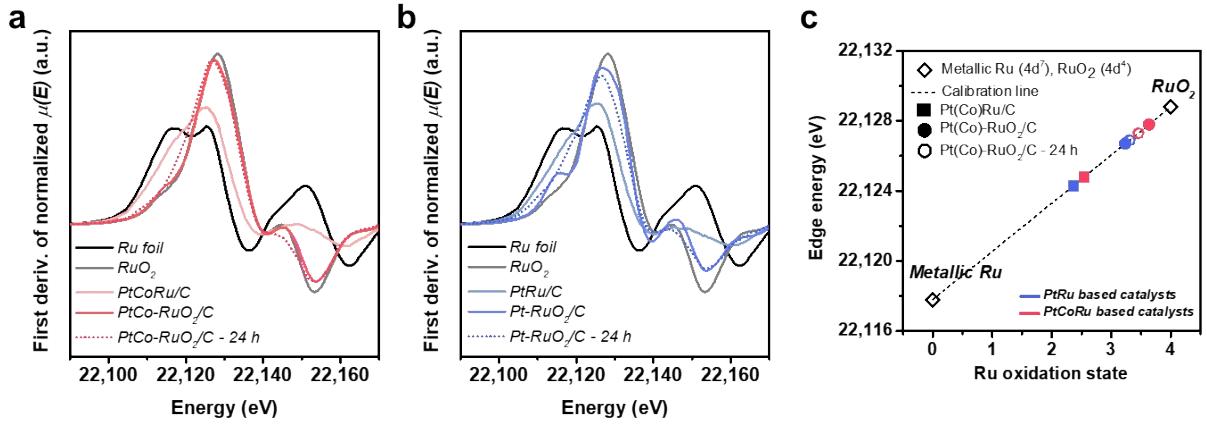

Fig. S26 First derivatives of Ru K-edge XANES regions of a) PtCo-RuO_2-based nanocatalysts and b) Pt-RuO_2-based nanocatalysts before and after thermal oxidation and OER stability test for 24 h. The edge energies of Ru were determined at the maximal values of the first derivatives of the XANES spectra. c) The edge energies for Ru K-edge as a function of the oxidation state of the Ru.

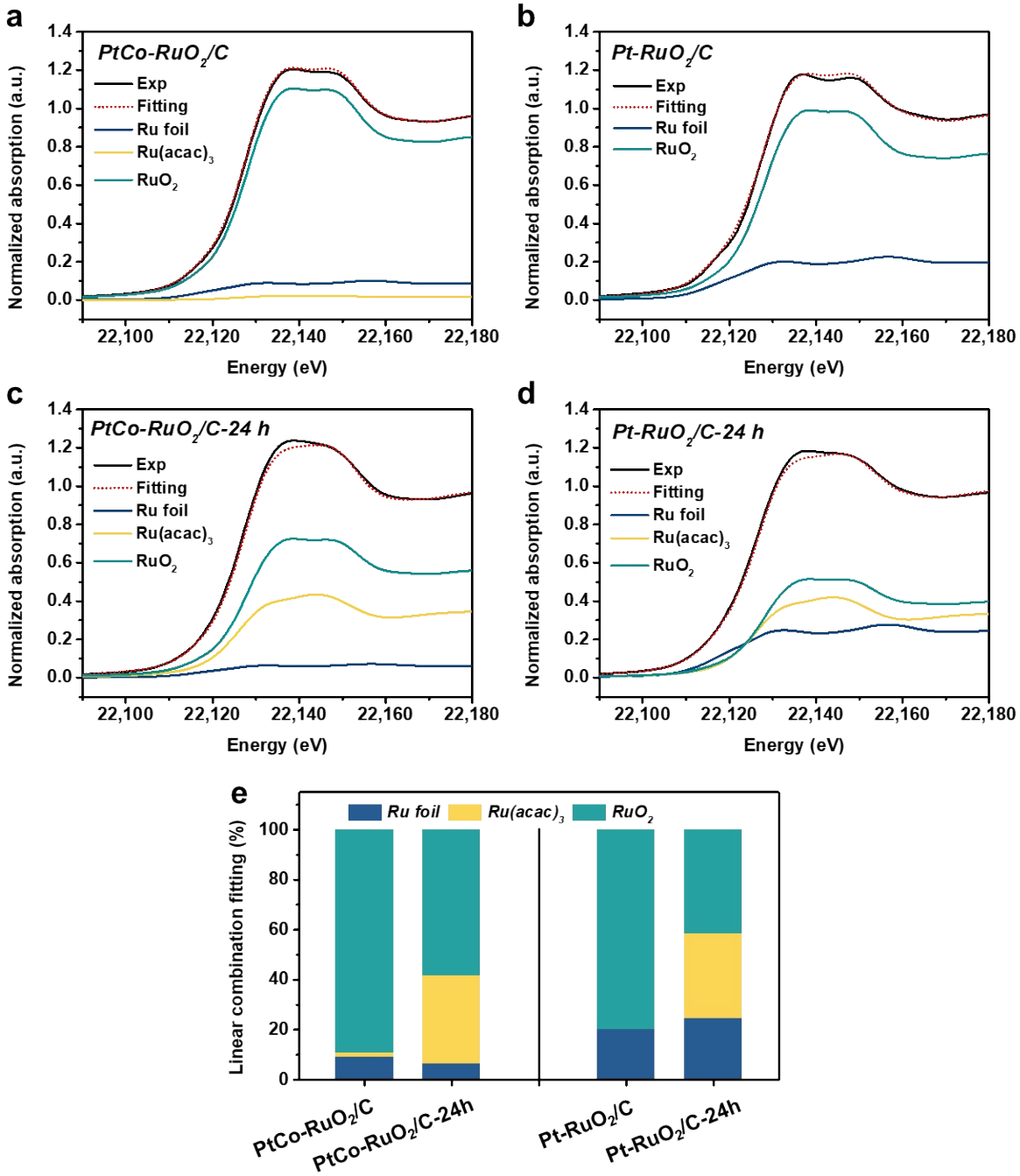

Fig. S27 Linear combination fitting of Ru K-edge XANES regions of a,c) PtCo-RuO_2-based nanocatalysts and b,d) Pt-RuO_2-based nanocatalysts before (a,b) and after OER stability test for 24 h (c,d). e) Area percentages of deconvoluted spectra based on above (a-d) results.

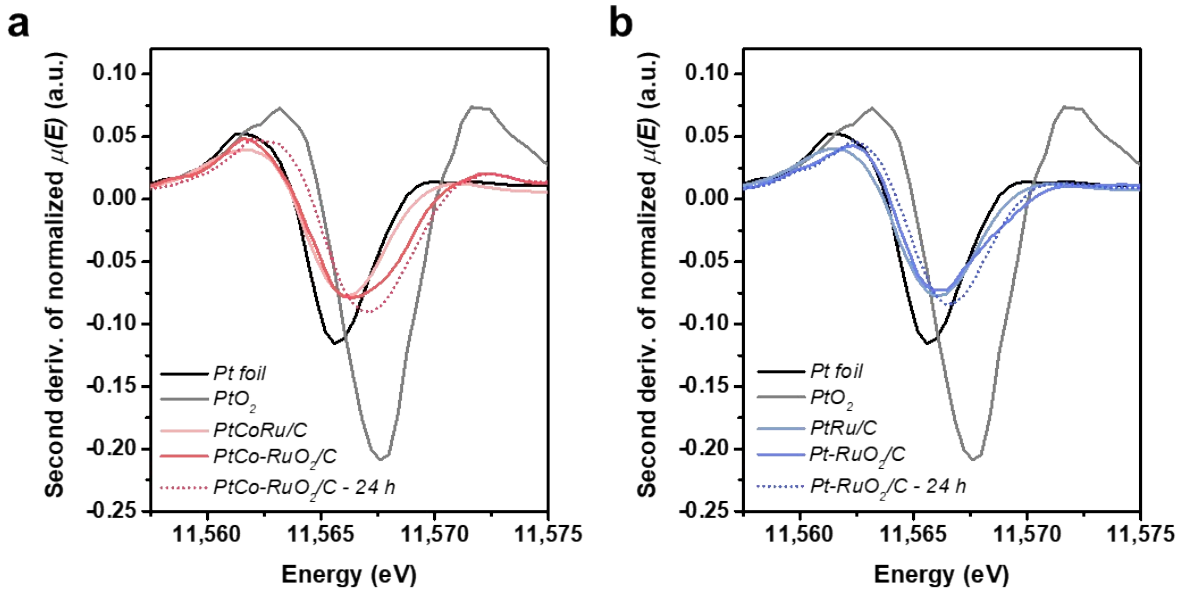

Fig. S28 Second derivatives of Pt L_3-edge XANES regions of a) PtCo-RuO_2-based nanocatalysts and b) Pt-RuO_2-based nanocatalysts before and after thermal oxidation and OER stability test for 24 h. The white line positions were determined at the minimal values of the second derivatives of the XANES spectra.

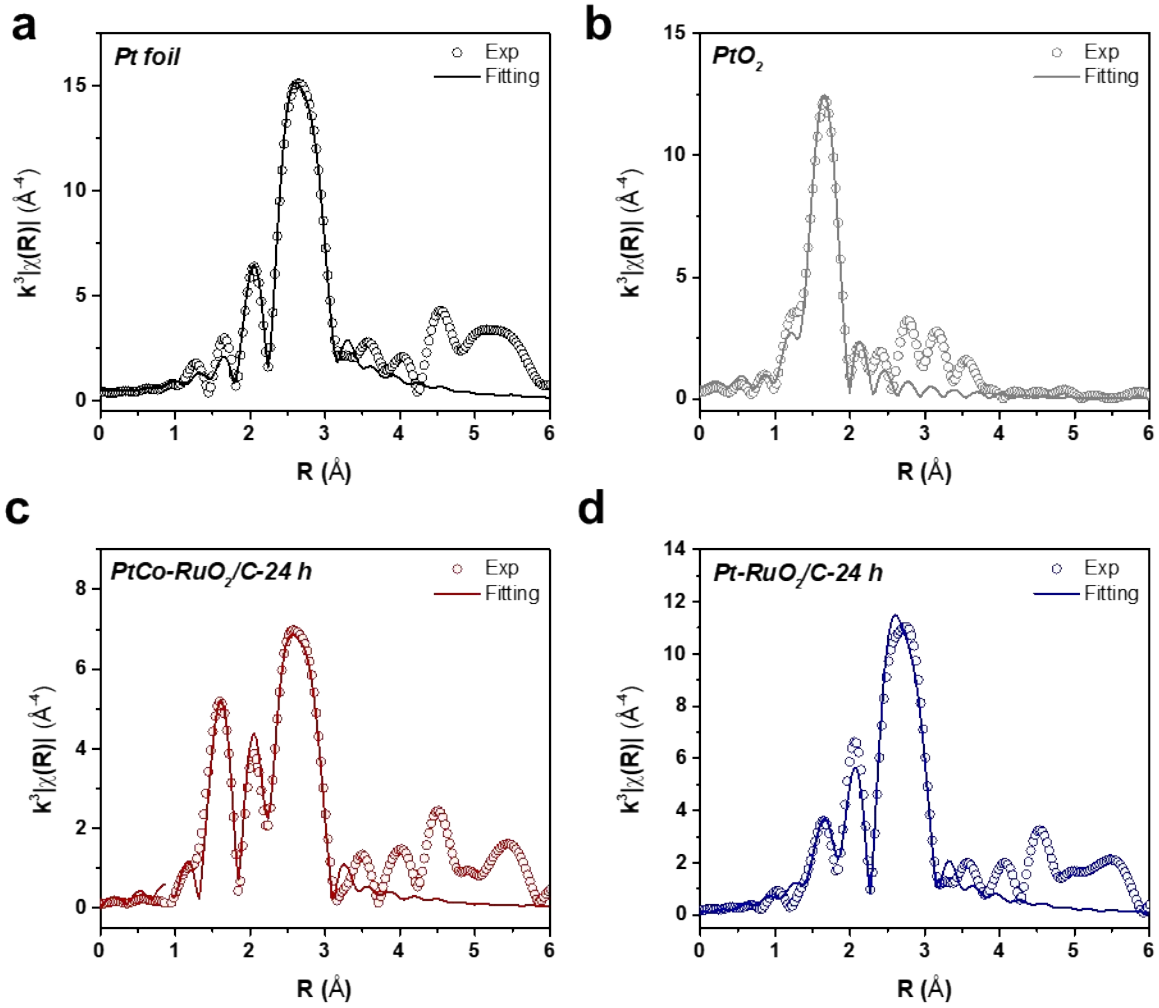

Fig. S29 Pt L_3-edge FT-EXAFS spectra in R-space with fitting curves of a) Pt foil (fitting range: R = 1.2-3.0 Å), b) PtO_2 (fitting range: R = 1.2-2.2 Å), c) PtCo-RuO_2/C-24 h (fitting range: R = 1.2-3.0 Å), and d) Pt-RuO2/C-24 h (fitting range: R = 1.2-3.0 Å).

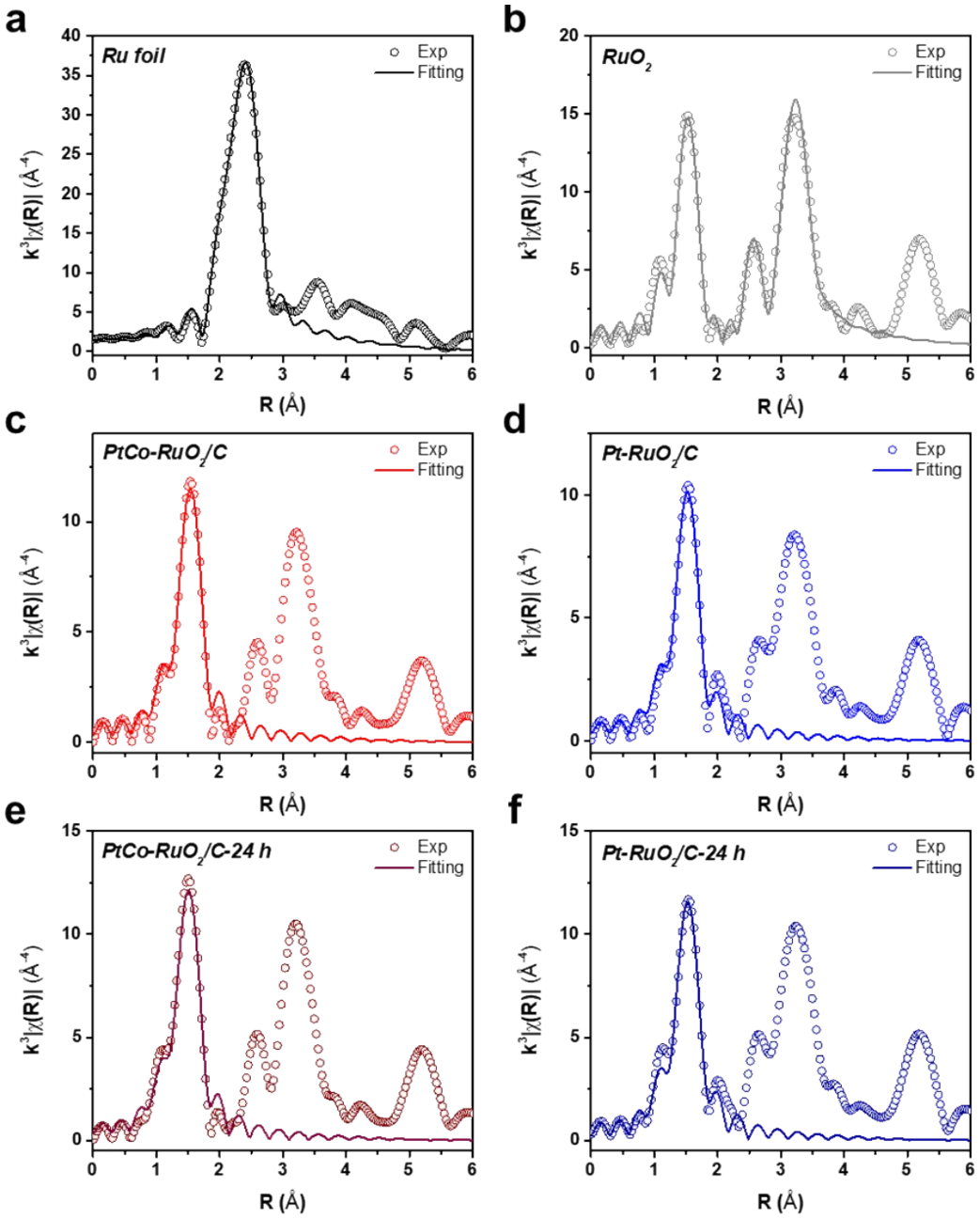

Fig. S30 Ru K-edge FT-EXAFS spectra in R-space with fitting curves of a) Ru foil (fitting range: R = 1.2-3.0 Å), b) RuO_2 (fitting range: R = 1.2-4.0 Å), c) PtCo-RuO_2/C (fitting range: R = 1.2-2.0 Å), d) Pt-RuO_2/C (fitting range: R = 1.2-2.0 Å), e) PtCo-RuO_2/C-24 h (fitting range: R = 1.2-2.0 Å), and f) Pt-RuO2/C-24 h (fitting range: R = 1.2-2.0 Å).

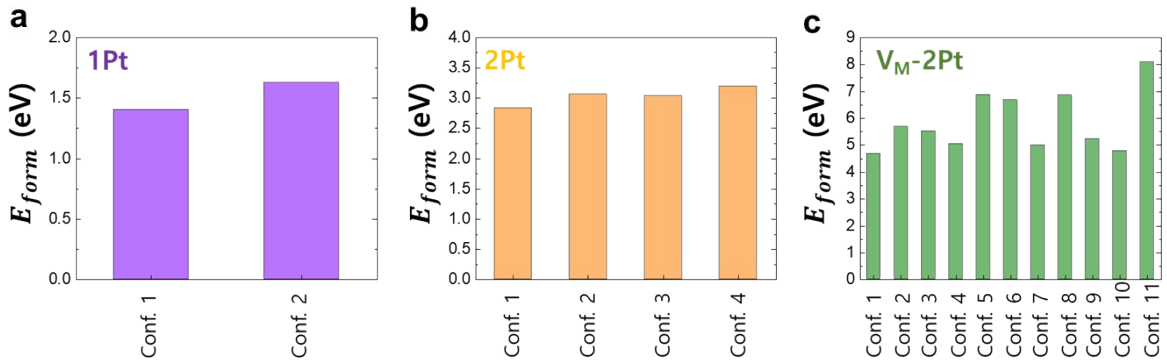

Fig. S31 The formation energies of various doping configurations for a) 1Pt, b) 2Pt, and c) V_M-2Pt.

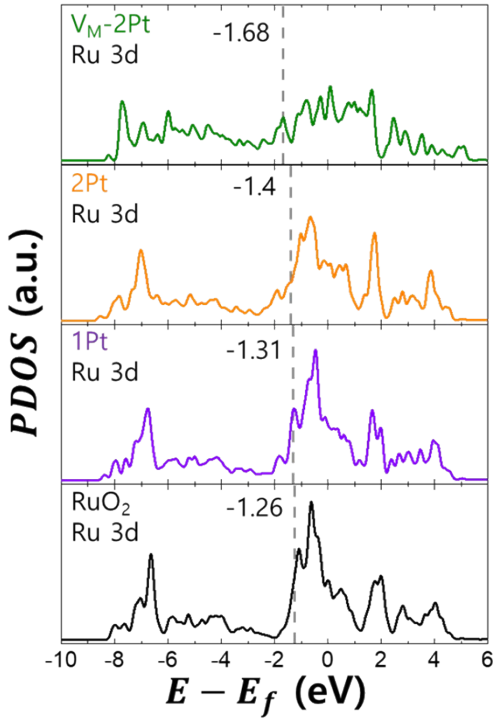

Fig. S32 PDOS of Ru_{cus} 3d-orbitals. The number represents the d-band center in each case.

Table S1 ICP-AES analysis results for contents for each metal in electrocatalysts.

Catalyst	Ru (wt%)	Pt (wt%)	Co (wt%)	Total (wt%)
Pt-RuO_2/C	7.17	16.05		23.22
PtCo-RuO_2/C	4.15	15.33	1.06	20.54

Table S2 Structural parameter of references (Pt foil and PtO_2) and catalysts from the EXAFS fitting for Pt L_3-edge. ($S_0^2 = 0.77$ obtained by the fitting of Pt foil was used to fit PtRu/C and PtCoRu/C and $S_0^2 = 0.66$ obtained by the fitting of PtO_2 was used to fit Pt-RuO_2/C-24 h and PtCo-RuO_2/C-24 h)

Sample	Scattering pair	*CN	R (Å)	σ^2 (10^{-3} Å^2)	ΔE_0 (eV)	R factor
Pt foil	Pt-Pt	12	2.77 ± 0.03	5.1 ± 0.1	8.14 ± 0.82	0.004
PtO_2	Pt-O	6	2.01 ± 0.07	2.2 ± 0.9	12.19 ± 1.66	0.008
PtRu/C	Pt-Ru	1.1 ± 0.7	2.72 ± 0.03	8.5 ± 4.7	7.80 ± 0.83	0.004
	Pt-Pt	9.7 ± 0.7	2.76 ± 0.01	6.0 ± 0.4		
PtCoRu/C	Pt-Co	2.4 ± 1.8	2.67 ± 0.05	13.9 ± 1.6	7.39 ± 1.23	0.004
	Pt-Ru	1.9 ± 0.8	2.74 ± 0.06	12.3 ± 1.7		
	Pt-Pt	6.5 ± 2.8	2.74 ± 0.01	5.2 ± 1.4		
PtCo-RuO_2/C-24 h	Pt-O	1.0 ± 0.4	1.98 ± 0.08	2.6 ± 1.9	5.04 ± 1.89	0.016
	Pt-Pt	11.3 ± 2.3	2.74 ± 0.09	8.1 ± 1.1		
Pt-RuO_2/C-24 h	Pt-O	0.2 ± 0.1	1.97 ± 0.15	8.0 ± 5.4	11.18 ± 2.25	0.0102
	Pt-Pt	10.5 ± 2.1	2.77 ± 0.01	5.2 ± 1.0		

*CN is the coordination number.

Table S3 Comparison of OER performance of present and reported Ru-based catalysts in acidic media.

Catalyst	Mass activity* ($A\ mg^{-1}_{Ru\ (Ir)}$)	Catalyst loading	η (mV) at 10 mA cm^{-2}	Electrolyte	Ref.
PtCo-RuO_2/C	7.552 @ 1.48 V_{RHE}	20 $\mu g_{Pt+Ru}\ cm^{-2}$	212	0.1 M $HClO_4$	This study
Pt-RuO_2/C	0.724 @ 1.48 V_{RHE}	20 $\mu g_{Pt+Ru}\ cm^{-2}$	274	0.1 M $HClO_4$	This study
RuO_2 NP/C	0.272 @ 1.48 V_{RHE}	20 $\mu g_{Ru}\ cm^{-2}$	265	0.1 M $HClO_4$	This study
com. RuO_2/C	0.034 @ 1.48 V_{RHE}	20 $\mu g_{Ru}\ cm^{-2}$	354	0.1 M $HClO_4$	This study
com. Ir/C	0.025 @ 1.48 V_{RHE}	20 $\mu g_{Ir}\ cm^{-2}$	324	0.1 M $HClO_4$	This study
RuO_2 NSs	0.516 @ 1.46 V_{RHE}	0.125 $\mu g\ cm^{-2}$	199	0.5 M H_2SO_4	[1]
Cu-doped RuO_2 (S-300)	-	275 $\mu g\ cm^{-2}$	188	0.5 M H_2SO_4	[2]
$Cr_{0.6}Ru_{0.4}O_2$ (550)	0.229 @ 1.5 V_{RHE}	-	178	0.5 M H_2SO_4	[3]
Mn-RuO_2	0.596 @ 1.5 V_{RHE}	275 $\mu g\ cm^{-2}$	158	0.5 M H_2SO_4	[4]
$Y_2Ru_2O_{7-\delta}$	-	-	190	0.1 M $HClO_4$	[5]
Ruthenate nanosheet	0.042 @ 1.48 V_{RHE}	200 $\mu g\ cm^{-2}$	255	0.1 M $HClO_4$	[6]
Co-RuO_2	-	-	169	0.5 M H_2SO_4	[7]
RuRh@(RuRh)O_2	0.437 @ 1.48 V_{RHE}	20.4 $\mu g_{metal}\ cm^{-2}$	245	0.1 M $HClO_4$	[8]
a-$RuTe_2$ PNRs	-	-	245	0.5 M H_2SO_4	[9]
$Ru_{0.9}Pt_{0.1}O_2$/C	-	24.6 $\mu g_{metal}\ cm^{-2}$	248	0.05 M H_2SO_4	[10]

Table S4 Comparison of PEMWE performance of present and reported electrocatalysts.

Catalyst (Anode)	Loading mass at anode (mg cm^{-2})	Cathode	Loading mass at cathode (mg cm^{-2})	Current density (A cm^{-2})	Cell voltage (V)	Ref.
PtCo-RuO_2/C	2.5	Pt/C (TKK) 46.5 wt%	0.25	4.4	2.0	This study
com. IrO_2	2.5	Pt/C (TKK) 46.5 wt%	0.25	3.7	2.0	This study
RuO_2 NS	2	Pt/C 47.1 wt%	1	0.93	1.65	[1]
Commercial RuO_2	2	Pt/C 47.1 wt%	1	0.31	1.65	[1]
Mg-doped $Y_2Ru_2O_7$ (YMRO-0.15)	3.9	Pt/C (TKK) 46 wt%	1.5	0.87	1.7	[11]
Commercial RuO_2	3.1	Pt/C (TKK) 46 wt%	1.5	0.39	1.7	[11]
$Y_{1.75}Ca_{0.25}Ru_2O_7$ (YCRO-0.25)	4.1	Pt/C	1.5	1.25	1.7	[12]
Commercial IrO_2	3	Pt/C	1.5	0.79	1.7	[12]
$Ir_{0.7}Ru_{0.3}O_2$	1.8	Pt/C	0.5	1	1.656	[13]
IrO_x calcined at 450 °C	2	Pt/C	0.5	1	1.680	[13]
SrRuIr	2	Pt/C 40 wt%	0.2	1	1.5	[14]

Table S5 Structural parameter of references (Ru foil and RuO_2) and catalysts from the EXAFS fitting for Ru K-edge. ($S_0^2 = 0.78$ was used to fit other catalysts)

Sample	Scattering pair	*CN	R (Å)	σ^2 (10^{-3} Å^2)	ΔE_0 (eV)	R factor
Ru foil	Ru-Ru_1	6	2.66 ± 0.96	2.7 ± 0.2	2.62 ± 1.90	0.002
	Ru-Ru_2	6	2.69 ± 0.84	4.2 ± 0.8		
RuO_2	Ru-O_1	6	1.99 ± 0.08	2.0 ± 0.1	1.64 ± 2.09	0.017
	Ru-Ru_1	2	3.12 ± 0.15	3.1 ± 0.2		
	Ru-O_2	4	3.37 ± 0.24	3.4 ± 0.2		
	Ru-Ru_2	8	3.58 ± 0.15	3.6 ± 0.2		
PtCo-RuO_2/C	Ru-O	5.2 ± 1.4	1.98 ± 0.15	2.2 ± 1.7	3.14 ± 4.14	0.014
Pt-RuO_2/C	Ru-O	4.6 ± 1.4	1.98 ± 0.17	2.3 ± 1.9	1.98 ± 4.72	0.017
PtCo-RuO_2/C-24 h	Ru-O	6.3 ± 0.1	1.97 ± 0.20	2.9 ± 1.1	1.55 ± 5.49	0.020
Pt-RuO_2/C-24 h	Ru-O	5.1 ± 1.2	1.98 ± 0.13	1.9 ± 1.5	0.90 ± 3.88	0.011

*CN is the coordination number.

Supporting References

[1] Z. L. Zhao, Q. Wang, X. Huang, Q. Feng, S. Gu, Z. Zhang, H. Xu, L. Zeng, M. Gu, and H. Li, *Energy Environ. Sci.*, 2020, **13**, 5143-5151

[2] J. Su, R. Ge, K. Jiang, Y. Dong, F. Hao, Z. Tian, G. Chen, and L. Chen, *Adv. Mater.,* 2018, 30, 1801351

[3] Y. Lin, Z. Tian, L. Zhang, J. Ma, Z. Jiang, B. J. Deibert, R. Ge, and L. Chen, *Nat. Commun.,* 2019, **10**, 162

[4] S. Chen, H. Huang, P. Jiang, K. Yang, J. Diao, S. Gong, S. Liu, M. Huang, H. Wang, and Q. Chen, *ACS Catal.,* 2020, 10, 1152-1160

[5] J. Kim, P.-C. Shin, K.-C. Tsao, Y.-T. Pan, X. Yin, C.-J. Sun, and H. Yang, *J. Am. Chem. Soc.*, 2017, **139**, 12076-12083

[6] S. Laha, Y. Lee, F. Podjaski, D. Weber, V. Duppel, L. M. Schoop, F. Pielnhofer, C. Scheurer, K. Müller, U. Starke, K. Reuter, B. V. Lotsch, *Adv. Energy Mater.,* 2019, **9**, 1803795

[7] Y. Tian, S. Wang, E. Velasco, Y. Yang, L. Cao, L. Zhang, X. Li, Y. Lin, Q. Zhang, and L. Chen, *iScience*, 2020, **23**, 100756

[8] K. Wang, B. Huang, W. Zhang, F. Lv, Y. Xing, W. Zhang, J. Zhou, W. Yang, F. Lin, P. Zhou, M. Li, P. Gao, and S. Guo, *J. Mater. Chem. A,* 2020, **8**, 15746-15751

[9] J. Wang, L. Han, B. Huang, Q. Shao, H. L. Xin, and X. Huang, *Nat. Commun.,* 2019, **10**, 5692

[10] J. Yi, W. H. Lee, C. H. Choi, Y. Lee, K. S. Park, B. K. Min, Y. J. Hwang, and H.-S. Oh, *Electrochem. Commun,* 2019, **104**, 106469

[11] Q. Feng, Z. Zhang, H. Huang, K. Yao, J. Fan, L. Zeng, M. C. Williams, H. Li, and H. Wang, *Chem. Eng. J.,* 2020, **395**, 124428

[12] Q. Feng, Z. Zhao, X.-Z. Yuan, H. Li, H. Wang, *Appl. Catal. B*, 2020, **260**, 118176

[13] M. Faustini, M. Giraud, D. Jones, J. Rozière, M. Dupont, T. R. Porter, S. Nowak, M. Bahri, O. Ersen, C. Sanchez, C. Boissière, C. Tard, J. Peron, *Adv. Energy Mater.,* 2019, **9**, 1802136

[14] Y. Wen, P. Chen, L. Wang, S. Li, Z. Wang, J. Abed, X. Mao, Y. Min, C. T. Dinh, P. D. Luna, R. Huang, L. Zheng, L. Wang, L. Wang, R. J. Nielsen, H. Li, T. Zhuang, C. Ke, O. Voznyy, Y. Hu, Y. Li, W. A. Goddard III, B. Zhang, H. Peng, and E. H. Sargent, *J. Am. Chem. Soc.,* 2021, **143**, 6482-6490